

A soft XAS transmission cell for operando studies

 Christoph Schwanke,[‡] Lifei Xi[‡] and Kathrin Maria Lange*

Operando Characterization of Solar Fuel Materials (EE-NOC), Helmholtz-Zentrum Berlin für Materialien und Energie, Albert-Einstein-Strasse 15, Berlin 12489, Germany. *Correspondence e-mail: kathrin.lange@helmholtz-berlin.de

Received 9 June 2016

Accepted 16 September 2016

Edited by R. W. Strange, University of Essex, UK

[‡] These authors contributed equally to this work.

Keywords: soft X-ray; transmission mode; manganese oxide; *in situ*; operando; *L*-edge.

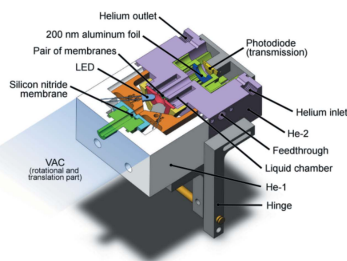
Supporting information: this article has supporting information at journals.iucr.org/s

A new cell for operando soft X-ray absorption spectroscopy in transmission mode is presented. Developed for investigations on solar water-splitting catalysts, the cell allows the study of solid films in direct contact with electrolyte solution while applying voltage and visible light. The design is optimized for fast sample exchange and the simultaneous measurement of fluorescence and transmission signal. The capability of the cell is presented on a manganese oxide (MnO_x) film, where electronic structure changes are monitored during forward and backward potential changes. Detailed information about the varying contributions of several Mn oxidation states during this process was revealed.

1. Introduction

For a knowledge-based optimization of functional materials such as, for example, catalysts, electronic structure investigations under realistic conditions are important. Since the active state of a catalyst in many cases only exists during the catalysis, operando characterization techniques are needed for a deep understanding of the catalysts structure–function correlation (Topsøe, 2003). For the study of solar water-splitting catalysts this requires a configuration in which the catalyst can be investigated in direct contact with an electrolyte solution.

Soft X-ray absorption spectroscopy (XAS) is an element-selective technique for investigating the *L*-edges of *3d* transition metals and the *K*-edges of the so-called life elements, nitrogen, oxygen and carbon (Lange *et al.*, 2012; Lange & Aziz, 2013). The transition metal *L*-edges are dominated by dipole-allowed transitions from occupied *2p* to unoccupied *3d* orbitals, which makes them well suited for investigating the partially unoccupied *3d* orbitals, which are pivotal for catalysis. Information on oxidation state, spin states and the interaction with ligands (charge transfer and backbonding) can be obtained. Indirect methods to measure XAS are widely applied. In one of those methods, total fluorescence yield (TFY) mode, all fluorescence photons resulting from the relaxation process after core-electron excitation are measured with a diode. This approach has the advantage that a sample thickness optimization is not required. It has been employed by a few groups (Guo, 2013; Braun *et al.*, 2012; Arthur *et al.*, 2012; Guay *et al.*, 2005; Bozzini *et al.*, 2014). However, TFY spectra can suffer from severe artefacts, for example the saturation or self-absorption effect, or can differ from the true absorption spectrum due to state-dependent decay probabilities (Nagasaka *et al.*, 2014; Schnohr & Ridgway, 2015; Turchini *et al.*, 1995; see also http://www-ssrl.slac.stanford.edu/mes/xafs/xas_intro.html). Furthermore, the signal intensity in TFY measurements is low, due to the low fluorescence yield in the soft X-ray regime. For example, at the Mn *L*₃-edge the



fluorescence yield is below 1% (Krause & Oliver, 1979). In order to obtain high signal intensities in TFY mode, a high intensity of the incoming X-ray beam is thus needed. However, this in turn can result in X-ray induced radiation damage. In contrast, measurements in transmission mode require lower light intensities and are suitable for obtaining true XAS spectra (Nagasaka *et al.*, 2014, 2010). However, measurements in transmission mode can be limited by the need for a sufficiently thin sample. Especially in the soft X-ray range this requirement can be difficult to fulfil, since attenuation lengths of solids are typically below 1 μm . For example, the attenuation length of Mn_2O_3 at 634 eV is 0.22 μm ([http://henke.](http://henke.lbl.gov/optical_constants/)

[http://henke.](http://henke.lbl.gov/optical_constants/)

To the best of our knowledge three groups have recently developed liquid cells for soft XAS in transmission mode (Nagasaka *et al.*, 2014, 2010; Schreck *et al.*, 2011; Huse *et al.*, 2009). In these designs X-rays are transmitted through the liquid which is confined by two ultrathin membranes. The liquid layer thickness is determined by the pressure of the surrounding gaseous helium (He) leading to bending of the ultrathin membranes. The cell of Huse *et al.* and Schreck *et al.* is optimized for measurements of liquids (Schreck *et al.*, 2011), whereas the design of Nagasaka *et al.* also allows operando characterization of solid/liquid electrochemical systems (Nagasaka *et al.*, 2014). Inspired by the work of Kosugi and co-workers (Nagasaka *et al.*, 2010) and our experience with operando spectroscopy (Schwanke *et al.*, 2014), we developed an operando soft X-ray transmission and fluorescence yield cell for the study of solid/liquid systems. Our design allows the sample to be manipulated by electrochemical techniques and visible light. It has the capability of sample exchange without breaking the high-vacuum conditions of the experimental

chamber and was optimized for fast sample exchange. Operando measurements, meaning in this case with applied voltage, are demonstrated here with a Mn *L*-edge study of an electrodeposited manganese oxide (MnO_x) film. Electrodeposited MnO_x films have attracted considerable attention as water oxidation catalyst, for supercapacitor and batteries due to their low cost, abundance, environmental friendliness and good electrochemical performance of the material (Xiao *et al.*, 2009; Tran *et al.*, 2015). We present here how the electronic structure changes of MnO_x can be monitored when going towards operando conditions and how detailed information on the oxidation state/configuration contribution can be obtained.

2. Results

2.1. Design of the soft XAS transmission flow cell for operando studies

A schematic illustration of the cell is given in Fig. 1. The setup consists of three chambers (VAC, He-1, He-2), of which VAC is evacuated and He-1 and He-2 are filled with He gas. A liquid under investigation or an electrolyte is confined between two Si_3N_4 membranes between He-1 and He-2. For operando measurements one of the membranes is coated with 20 nm Au and the sample film. The Au provides the necessary conductivity.

For a transmission measurement soft X-rays from a beamline pass through chamber VAC into chamber He-1, are partially absorbed by the liquid–solid sample system, and are detected with a GaAsP photodiode (Hamamatsu G1127) in chamber He-2. At the same time fluorescence photons can be detected with two photodiodes (Hamamatsu G1127) in

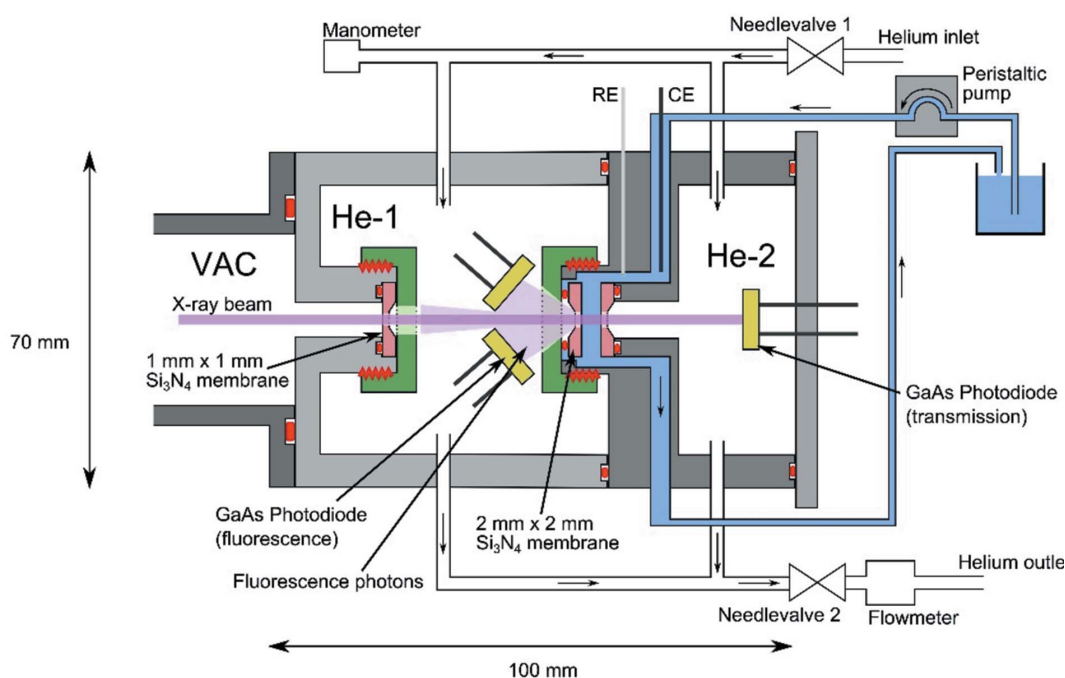


Figure 1
Schematic illustration of the soft X-ray transmission cell.

chamber He-1 providing absorption-like spectra in TFY mode. The liquid layer thickness can be tuned by the He pressure in chambers He-1 and He-2 (Huse *et al.*, 2009; see also http://henke.lbl.gov/optical_constants/). Reference electrode and counter electrode are placed in the electrolyte close to the Au-coated membrane, which serves as a working electrode. Visible light can be applied to the cell with two LEDs, which can be placed in He-1 instead of the TFY diodes. If visible light is used, a 200 nm-thick Al foil in He-2 blocks the visible light from the photodiode in He-2.

The chambers VAC and He-1 are separated by a 1 mm × 1 mm × 100 nm Si₃N₄ membrane and the chambers He-1 and He-2 are separated by a pair of 2 mm × 2 mm × 100 nm Si₃N₄ membranes (Silson Ltd). The frames of the pair of membranes are separated by 100 μm PTFE spacers and the solid/liquid system under investigation is confined in this space. The He pressure can be regulated *via* two needle valves: one between the He source and the cell and one before the outlet of the He system after the cell. Positioning of the cell is performed by a translational stage and an angular stage (see Fig. S1 of the supporting information).

In order to minimize the time for replacing samples or broken membranes, caps are designed with one single thread (see Fig. S2 of the supporting information). Between the liquid chamber and the cap a part is introduced to prevent the membranes from rotating while the cap is turned (see Fig. S2). A further reduction of the number of loose parts compared with previous cell designs is achieved by the use of a hinge and a lever to grant access to the membranes (see Fig. 2 for a 3D model).

The advantages of this cell design for the study of solids, liquids and solid/liquid interfaces under operando conditions (applied voltage/light illumination) are: (i) the possibility to measure XAS in transmission and fluorescence mode simultaneously, (ii) fast sample/membrane replacement (less than 5 min), (iii) reduced risk of beamline contamination with

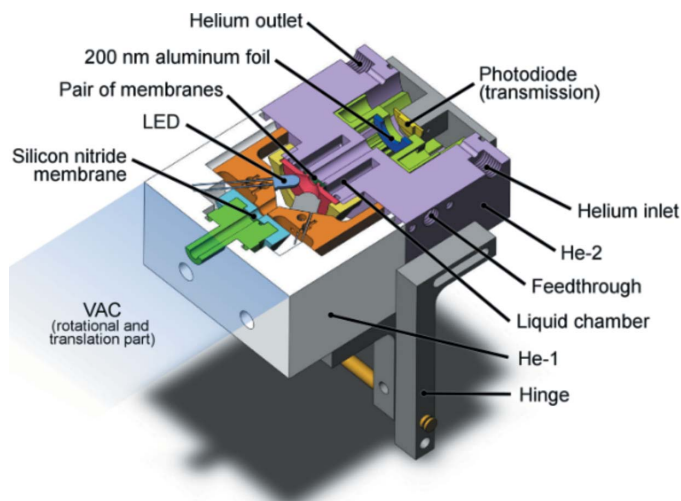


Figure 2
Schematic illustration (3D model) of the soft X-ray transmission cell. Here, two white LEDs are used to illuminate a photoanode. A 200 nm-thick aluminium foil is put in front of the photodiode in region He-2 to block the visible light from the LEDs.

electrolyte solution due to two protection membranes, and (iv) manipulation of the sample with visible light.

2.2. Proof of principle: Mn *L*-edge spectra of a MnO_x film under varying potentials

Here we present the effect of applied potential on the electronic structure of an electrodeposited MnO_x film measured in transmission mode. Forward and backward scans were carried out in order to reveal dependencies on the direction of potential sweep. The Mn *L*-edge spectra of the MnO_x film (~200 nm thick) are presented in Fig. 3, where the spectral features are labelled from *a* to *h*. In the spectra a clear dependency on potential as well as on potential test direction can be observed. Upon comparison with the reference spectra the features *b*, *d* and *f* can be assigned to Mn²⁺, Mn³⁺ and Mn⁴⁺, respectively. Peak *c* at 641.3 eV possibly has the same origin as in Mn₃O₄, indicating a similar structure (Khan *et al.*, 2015).

In order to reveal the contributions from different Mn oxidation states, linear combination fitting of the spectra was carried out. For this purpose spectra recorded in total electron yield (TEY) mode of reference powders of the expectable MnO_x oxidation states MnO (II), Mn₂O₃ (III) and MnO₂ (IV) were used, which were previously published (see Fig. S3) (Khan *et al.*, 2015). Spectra recorded in TEY mode are considered close to true XAS spectra since they are weakly influenced by self-absorption effects (Nakajima *et al.*, 1999). A typical fit is shown in Fig. 4. The quality of the fit is quite good, but deviations occur between experimental spectra and fit. The deviations could indicate that the reference spectra recorded from powder samples do not fully represent the electronic structure of the investigated MnO_x (Datta *et al.*, 2012). In Fig. 5 the results of the linear combination fitting analysis are presented. In the forward scan the fractions of Mn³⁺ and Mn⁴⁺ increase while the amount of Mn²⁺ decreases. With the here-presented fractional distribution of oxidation

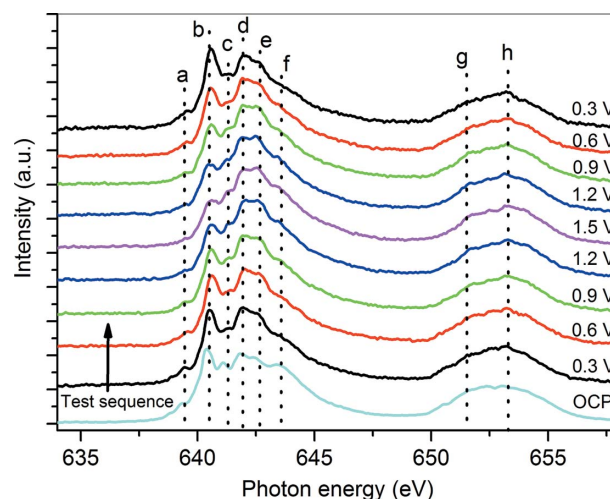


Figure 3
XAS spectra of MnO_x in 0.1 M KP_i buffer solution under different potentials.

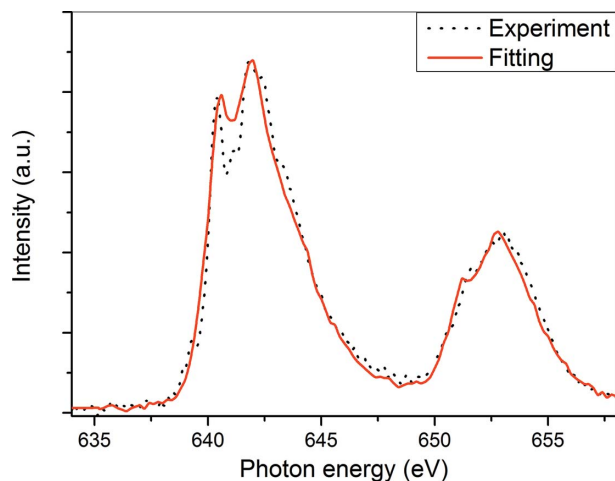


Figure 4
Linear combination fitting of Mn *L*-edge spectra of the MnO_x films under 0.6 V versus NHE in 0.1 M KPi from the backward scan.

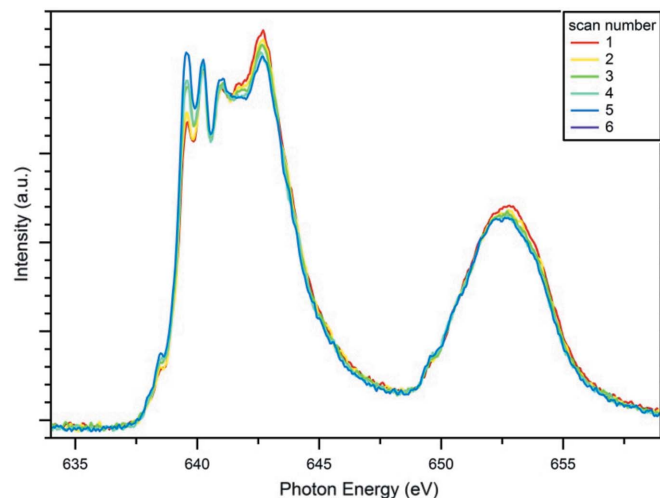


Figure 6
Repeated measurements of the MnO_x film while no liquid layer was present. The variations are assigned to be beam induced. Each scan took 5 min, and per scan a dose of 11.7 MGy was absorbed by the film, much more than in the other spectra in this publication (0.26 MGy per scan).

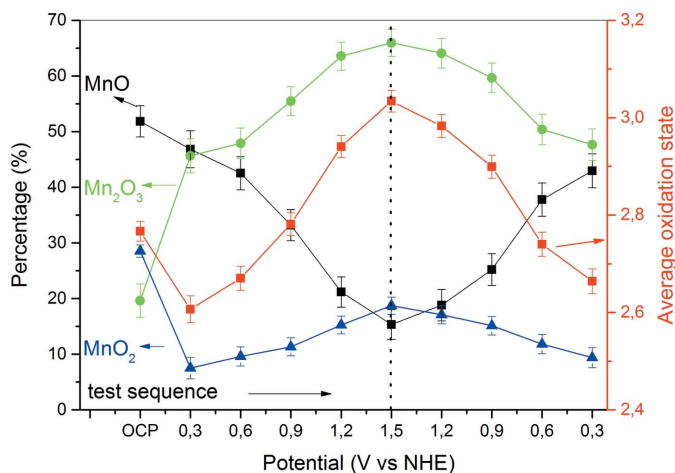


Figure 5
Contributions from the reference manganese oxide species MnO , Mn_2O_3 and MnO_2 to the MnO_x film upon varying potential obtained *via* linear combination fitting. The resulting change of the overall oxidation state of MnO_x under different potentials is shown in red. The order of the test sequence is marked in the graph with an arrow.

state species under operando conditions, correlations to the catalytic active species can be made, which will be the topic of further investigations. Note that, in the reverse scan, a delay or hysteresis of oxidation state change is found compared with the forward scan. This phenomenon was previously observed by several groups when studying the oxygen evolution catalysts CoO_x (Risch *et al.*, 2015) and nickel borate (NiB_i) (Yoshida *et al.*, 2015). Such a delayed transition was proposed to be related to the asymmetry of the oxidation of surface and bulk on forward and backward scan as found in metal oxides nanoclusters (Yoshida *et al.*, 2015). In this model it was assumed that the observed oxidation states changes take place in the bulk of the material. This assumption is also supported by a linear relation between layer thickness and activity which was found in a class of hydroxide-like cobalt OER catalysts (cobalt phosphate, Co-P_i , and cobalt borate, Co-B_i) (Esswein *et al.*, 2011; Klingan *et al.*, 2014). The here-observed rather

large percentage of Mn atoms that change oxidation state considering the film thickness of about 200 nm and the hydroxide-like nature of the material hints also at oxidation state changes throughout the whole film.

It has to be mentioned that the here-obtained average oxidation states lie significantly below values obtained from coulometry measurements (Huynh *et al.*, 2014), which could be explained by radiation-induced reduction of the sample. During the measurement, radiation damage is actually greatly suppressed, since absorption in the liquid layer reduces the intensity of the incoming X-ray beam before interacting with the sample. Depending on the liquid layer thickness the photon flux reaching the sample can be tuned. For our settings, which are listed in the supporting information, we estimated a dose of 0.26 MGy per scan, taking 5 min. Details on the calculation of the dose can be found in the supporting information. In total the whole dataset was recorded in about 150 min.

However, in the here-presented dataset the sample was exposed to the X-rays without liquid in the cell before the data acquisition, leading to a reduction of the sample. Without liquid, a clear indication of the reduction of Mn can be seen already after one scan as given in Fig. 6. During one scan (5 min) a dose of 11.7 MGy (no liquid) was deposited. A total of six scans were recorded, resulting in a dose of 70.2 MGy and a significant alteration of the XAS spectrum. The here-reported dose can be compared with organic polymers investigated at the carbon 1s edge (280 eV), where doses of the order of 50–100 MGy were found to lead to significant radiation damage (Leontowich *et al.*, 2016).

3. Conclusion

We reported a new design of an operando soft X-ray transmission and fluorescence cell with the capability of fast membrane replacement and easy operation compared with

previous designs. The cell is suitable for studying solids, liquids and solid/liquid interfaces and manipulating the sample with electrochemical techniques and visible light. For the proof of concept, XAS spectra of the Mn *L*-edge of MnO_x films were measured under operando conditions.

4. Related literature

The following references are cited in the supporting information: Krumrey & Tegele (1992), Leontowich *et al.* (2012) and Ruosi *et al.* (2014).

Acknowledgements

We thank Professor Nobuhiro Kosugi and Dr Masanari Nagasaka for valuable discussions and Mr Ivo Rudolph for the preparation of the Au coatings. This work was supported by the Helmholtz Association (VH-NG-1140).

References

Arthur, T. S., Glans, P. A., Matsui, M., Zhang, R., Ma, B. & Guo, J. (2012). *Electrochem. Commun.* **24**, 43–46.

Bozzini, B., Gianoncelli, A., Bocchetta, P., Dal Zilio, S. & Kourousias, G. (2014). *Anal. Chem.* **86**, 664–670.

Braun, A., Sivula, K., Bora, D. K., Zhu, J., Zhang, L., Grätzel, M., Guo, J. & Constable, E. C. (2012). *J. Phys. Chem. C*, **116**, 16870–16875.

Datta, S., Rule, A. M., Mihalic, J. N., Chillrud, S. N., Bostick, B. C., Ramos-Bonilla, J. P., Han, I., Polyak, L. M., Geyh, A. S. & Breysse, P. N. (2012). *Environ. Sci. Technol.* **46**, 3101–3109.

Esswein, A. J., Surendranath, Y., Reece, S. Y. & Nocera, D. G. (2011). *Energy Environ. Sci.* **4**, 499.

Guay, D., Stewart-Ornstein, J., Zhang, X. & Hitchcock, A. P. (2005). *Anal. Chem.* **77**, 3479–3487.

Guo, J. (2013). *J. Electron Spectrosc. Relat. Phenom.* **188**, 71–78.

Huse, N., Wen, H., Nordlund, D., Szilagy, E., Daranciang, D., Miller, T. A., Nilsson, A., Schoenlein, R. W. & Lindenberg, A. M. (2009). *Phys. Chem. Chem. Phys.* **11**, 3951–3957.

Huynh, M., Bediako, D. K., Liu, Y. & Nocera, D. G. (2014). *J. Phys. Chem. C*, **118**, 17142–17152.

Khan, M., Xiao, J., Zhou, F., Yablonskikh, M., MacFarlane, D. R., Spiccia, L. & Aziz, E. F. (2015). *ChemSusChem*, **8**, 1980–1985.

Klingan, K., Ringleb, F., Zaharieva, I., Heidkamp, J., Chernev, P., Gonzalez-Flores, D., Risch, M., Fischer, A. & Dau, H. (2014). *ChemSusChem*, **7**, 1301–1310.

Krause, M. O. & Oliver, J. H. (1979). *J. Phys. Chem. Ref. Data*, **8**, 329.

Krumrey, M. & Tegeler, E. (1992). *Rev. Sci. Instrum.* **63**, 797–801.

Lange, K. M. & Aziz, E. F. (2013). *Chem. Soc. Rev.* **42**, 6840–6859.

Lange, K. M., Kothe, A. & Aziz, E. F. (2012). *Phys. Chem. Chem. Phys.* **14**, 5331–5338.

Leontowich, A. F. G., Hitchcock, A. P. & Egerton, R. F. (2016). *J. Electron Spectrosc. Relat. Phenom.* **206**, 58–64.

Leontowich, A. F. G., Hitchcock, A. P., Tyliszczak, T., Weigand, M., Wang, J. & Karunakaran, C. (2012). *J. Synchrotron Rad.* **19**, 976–987.

Nagasaka, M., Hatsui, T., Horigome, T., Hamamura, Y. & Kosugi, N. (2010). *J. Electron Spectrosc. Relat. Phenom.* **177**, 130–134.

Nagasaka, M., Yuzawa, H., Horigome, T. & Kosugi, N. (2014). *Rev. Sci. Instrum.* **85**, 104105.

Nakajima, R., Stöhr, J. & Idzerda, Y. U. (1999). *Phys. Rev. B*, **59**, 6421–6429.

Risch, M., Ringleb, F., Kohlhoff, M., Bogdanoff, P., Chernev, P., Zaharieva, I. & Dau, H. (2015). *Energ. Environ. Sci.* **8**, 661–674.

Ruosi, A., Raisch, C., Verna, A., Werner, R., Davidson, B. A., Fujii, J., Kleiner, R. & Koelle, D. (2014). *Phys. Rev. B*, **90**, 125120.

Schnohr, C. S. & Ridgway, M. C. (2015). Editors. *X-ray Absorption Spectroscopy of Semiconductors, Springer Series in Optical Sciences 190*. Berlin/Heidelberg: Springer-Verlag.

Schreck, S., Gavril, G., Weniger, C. & Wernet, P. (2011). *Rev. Sci. Instrum.* **82**, 103101.

Schwanke, C., Golnak, R., Xiao, J. & Lange, K. M. (2014). *Rev. Sci. Instrum.* **85**, 103120.

Topsøe, H. (2003). *J. Catal.* **216**, 155–164.

Tran, M. V., Ha, A. T. & Le, P. M. L. (2015). *J. Nanomater.* **2015**, 609273.

Turchini, S., Delaunay, R., Lagarde, P., Vogel, J. & Sacchi, M. (1995). *J. Electron Spectrosc. Relat. Phenom.* **71**, 31–37.

Xiao, F., Xu, Y. & Bai, H. (2009). *Int. J. Electrochem. Sci.* **248**, 6671.

Yoshida, M., Mitsutomi, Y., Mineo, T., Nagasaka, M., Yuzawa, H., Kosugi, N. & Kondoh, H. (2015). *J. Phys. Chem. C*, **119**, 19279–19286.